SCIENCE CHINA
Earth Sciences

•RESEARCH PAPER•

November 2018 Vol.61 No.11: 1644–1658
https://doi.org/10.1007/s11430-017-9236-7

Influence of mantle convection to the crustal movement pattern in the northeastern margin of the Tibetan Plateau based on numerical simulation

Aiyu ZHU[1], Dongning ZHANG[1,2*], Tao ZHU[1] & Yingxing GUO[1]

[1] *Institute of Geophysics, China Earthquake Administration, Beijing 100081, China;*
[2] *Key Laboratory of Seismic Observation and Geophysical Imaging, Institute of Geophysics, China Earthquake Administration, Beijing 100081, China*

Received September 11, 2017; revised June 4, 2018; accepted June 12, 2018; published online September 27, 2018

Abstract Based on the recent observations about the movement and rheological structure of the lithosphere and deformation pattern of the crust, we developed a three-dimensional finite element model for the northeastern margin of the Tibetan Plateau. The model considered the impacts of both external and internal conditions, including mantle convection, gravitational potential energy and block interactions. We compared the simulated surface movement rates to the observed GPS velocities, and the results revealed that crustal movement gradually decreased toward the edge of the plateau. The factors controlling this pattern are the interactions of adjacent blocks, gravitational potential energy of the plateau, and also mantle convection as well. Additionally, according to the observation that there was an apparent difference between the horizontal movement rate of the lithosphere and convective velocity of the underlying mantle, and also based on the results of seismic anisotropy studies that suggest different strengths and deformation regimes of the lithosphere in different tectonic blocks, we proposed that the impact of mantle convection on the lithosphere may have varied in space, and introduced a parameter named mantle convection intensity factor in numerical simulations. Our simulation results show consistent surface movement rates with GPS observations, which further supports the viewpoint of seismic anisotropy studies, i.e., the degree of coupling between the crust and mantle varies significantly among different blocks.

Keywords Northeastern margin of the Tibetan Plateau, Crustal movement, Mantle convection, Numerical simulation

Citation: Zhu A, Zhang D, Zhu T, Guo Y. 2018. Influence of mantle convection to the crustal movement pattern in the northeastern margin of the Tibetan Plateau based on numerical simulation. Science China Earth Sciences, 61: 1644–1658, https://doi.org/10.1007/s11430-017-9236-7

1. Introduction

The northeastern margin of the Tibetan Plateau (Figure 1) is a convergence zone, which is composed of the actively crustal deforming plateau, and the more tectonically stable Alashan block, Erdos block, and Huanan block (Zhang et al., 2003; Yuan et al., 2004). Based on the results of GPS observation (Fang et al., 2009; Cui et al., 2009; Li et al., 2012; Liang et al., 2013; Ge et al., 2013; Li et al., 2015) and the geological investigation (Yuan et al., 2004; Zhang et al., 2013; Hao et al., 2014), it has been demonstrated that crustal movement of the northeastern margin of the Tibetan Plateau is gradually decreasing from the top of the plateau to its edge, and there are obvious differences between the eastern and the western edges. The main kinetic control factors in the dynamic model of current crustal movement patterns in the northeastern margin of the Tibetan Plateau are considered as follows: the high altitude terrain of the plateau, interactions between the Indian plate and Eurasian plate, differences in the tectonic characteristics and mechanical properties of the

* Corresponding author (email: zhangdn@cea-igp.ac.cn)

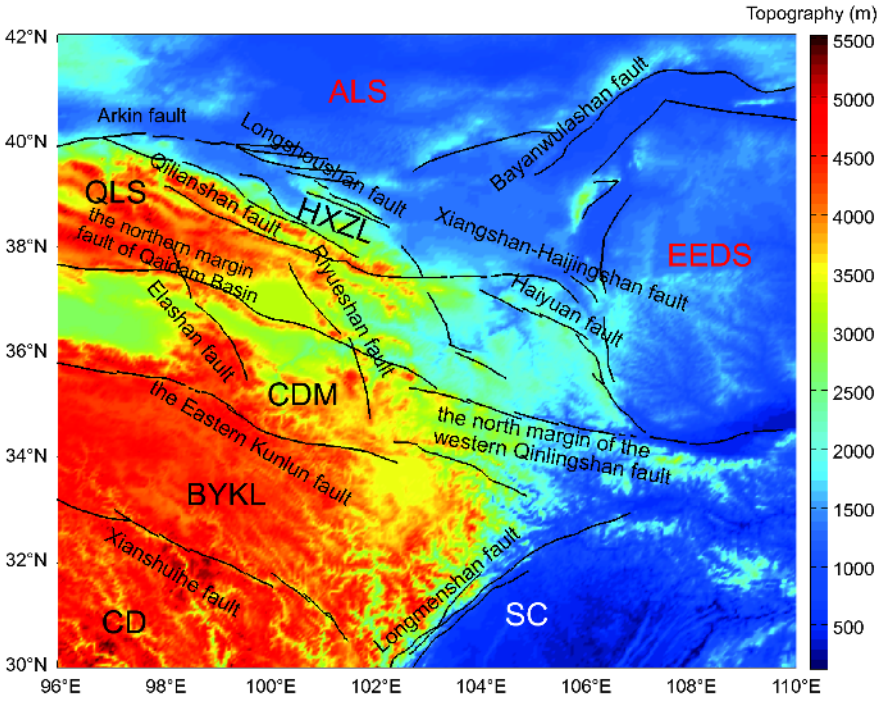

Figure 1 Geological structure of the eastern margin of the Tibetan Plateau. The background is the terrain height in meters; SC is the Sichuan basin, CD is the Sichuan-Yunnan block, BYKL is the Bayanhar block, CDM is the Qaidam block, QLS is the Qilianshan block, EEDS is the Erdos block, ALS is the Alashan block, and HXZL is the Hexi Corridor basin.

deep and shallow parts of the crust, and mantle convection at the bottom of lithosphere (Liu and Yang, 2003; Bird et al., 2008; Becker and Faccenna, 2011; Faccenna et al., 2013; Chen et al., 2017).

With the development of the lithospheric geodynamics of the Tibetan Plateau, the control effect of the mantle convection at the bottom of lithosphere on the tectonic movement attracted much attention, in addition to the above kinetic factors (Fu et al., 1998, 2005; Bird, 1999; Xiong and Teng, 2002; Xiong et al., 2005, 2010; Huang and Zhong, 2005; Zhu, 2014, 2016). Bird et al. (2008) analyzed various dynamic factors that drive the plate movements and stress states of the lithosphere, and results of their numerical simulation revealed that plate motion is dominantly driven by deep mantle convection, the influence of which is greater than those of both crustal topography and the lithostatic pressure of the lithosphere. Huang et al. (2008) simulated the crustal deformation field of the northeastern margin of the Tibetan Plateau, and the results indicated that simulation results more closely mirror GPS observations when two kinds of loading conditions are considering together, such as the pushing force from the plate and mantle convection at the bottom of lithosphere. Zhang et al. (2007) arrived at similar conclusions to those of Huang et al. (2008) when they conducted numerical simulations on the crustal movement of the Tibetan Plateau. Because of the complex geologic structure of the Tibetan Plateau, the simulation results differed from those derived from GPS observations (Zhang et al., 2007; Huang et al., 2008). To reduce the differences between the simulations and the GPS observations, the numerical model itself as well as the dynamic boundary conditions that more closely approximate the real lithospheric environment must be considered. In recent years, more reliable mantle convection data (Zhu, 2016), which can help us to improve the accuracy of simulation results, have been obtained through seismic tomography observations. Based on this new data, we analyzed the effects of mantle convection to the crustal movement pattern on the northeastern margin of the Tibetan Plateau by three-dimensional finite element modeling.

So far the results of small-scale mantle convection simulations in the Tibetan Plateau were very different because of the different methods and data sources utilized. Using regional isostatic gravity anomaly data, Fu et al. (1998) derived a small-scale convection model of upper mantle in the central and northern areas of Tibetan Plateau to the areas of Tianshan. Xiong and Teng (2002) and Xiong et al. (2005) then obtained the stress field of convection in the Tibetan Plateau and its adjacent area using the Bouguer gravity anomaly. In recent years, a new method for calculating mantle convection has been developed using seismic tomography data. By using this method, as well as considering the lateral inhomogeneity of the mantle viscosity coefficient, the mantle convection model has proven to be more consistent with the observed plate movement (Fu et al., 2003). Zhu (2016) established a small-scale mantle convection model based on seismic tomography, and investigated the influence of mantle con-

vection to the lithospheric stress field of the Chinese continent. In the establishment of this mantle convection model, Zhu (2016) took into account the local-scale of seismic tomography models in order to describe the mantle structure in the horizontal direction with a higher degree of resolution. In this latest model, tomography data with local-scale resolution were selected as much as possible, and global scale tomography models were used in some poor detection areas (see Steinberger et al., 2001 for a useful discussion). However, the methods and principles employed in these studies were different, so the small-scale mantle convection images obtained also differed. After comparative analysis of these results, we elected to use the latest mantle convection model of Zhu (2016).

In this study, we present a numerical model for exploring the crustal movement patterns of the northeastern margin of the Tibetan Plateau, and consider the internal and external dynamic factors influencing these patterns, including the gravitational potential energy accumulated in high altitude terrain, plate interactions, and mantle convection at the bottom of the lithosphere. Most of numerical geodynamic models of the Tibetan Plateau developed previously have directly applied mantle convention at the bottom of the model without considering the interactions between the lithosphere and the underlying mantle. However, recent studies have suggested that this interaction significantly influenced the actual mantle convection (Zhu, 2017). Considering this interaction, Bourne et al. (1998) proposed that the crust can withstand the forces of underlying rock layers in proportion to the horizontal velocity of upper and lower layers of the crust. According to the seismic anisotropy research of Chang et al. (2017), the strength of the vertical coherence deformation is also significantly different in the Tibetan Plateau and its adjacent areas, and this may also be related to the differences observed in the degree of coupling degree between the lithosphere and the asthenosphere. Therefore, if we simply apply the mantle convection to the bottom of the numerical model, the results may greatly deviate from physical reality.

Based on this previous research, we propose here that the intensity of mantle convection differs between the center and the northeastern margin of the Tibetan Plateau and its adjacent blocks, and we apply this assumption to our numerical simulations. We apply different proportions of mantle convection at the bottom of different blocks, and then compare different loading schemes, including different proportions of mantle convection at the bottom of different blocks, and without mantle convection at the bottom of the lithosphere. In order to explore whether mantle convection imposes a dominant control on the deformation of the northeastern margin of the Tibetan Plateau, and to better understand how it controls patterns of crustal movement, we analyze the consistency between the simulated results of crustal deformation and GPS observation. Our results provide a quantitative dynamic framework for analyzing seismic hazards in this area.

2. Three-dimensional finite element modeling

2.1 Model geometry

Based on the latest data on the velocity structure and physical parameters of the northeastern margin of the Tibetan Plateau, we established a three-dimensional viscoelastic finite element model (Stolk et al., 2013; Li et al., 2013; Xu et al., 2014). The study area extends from 96°E to 110°E and from 30°N to 42°N (Figure 2), and the model included many active blocks, such as the Erdos block, the Sichuan basin, the Alashan block, then Qilianshan block, the Qaidam block, the Bayanhar block, the Sichuan-Yunnan block, and others.

The model used also included many active faults: the Arkin fault zone, the Qilianshan fault zone, the Bayanwulashan fault, the Haiyuan fault zone, the north margin of the western Qinlingshan fault zone, the Riyueshan fault zone, the Elashan fault zone, Xiangshan-Tianjingshan fault, the northern margin fault of Qaidam basin, the Longshoushan Fault zone, the Eastern Kunlun fault zone, the Xianshuihe fault zone, and the Longmenshan fault zone (Yuan et al., 2004). The Qilianshan fault as well as the north margin of the Qaidam basin fault and Haiyuan fault are thrust zones. The dip angle was 60° and the width was 20 km in the model. The Longmenshan fault zone on the edge of the Tibetan Plateau was simplified (i.e., the back range fault, the central fault, and the front range fault were simplified as a fault zone with a width of 40 km), and the dip angle of the fault zone was close to the source mechanism of the M_S8.0 Wenchuan earthquake in 2008 (Chen et al., 2013). The depth of this fault is 20 km according to seismic detection, magnetotelluric (MT) sounding, and seismic location (Teng et al., 2008). The rest of the study faults are strike slip faults for which we set a vertical dip angle and a width of 10 km, according to previous results. Some researchers believe that the discontinuous contact elements can better describe the

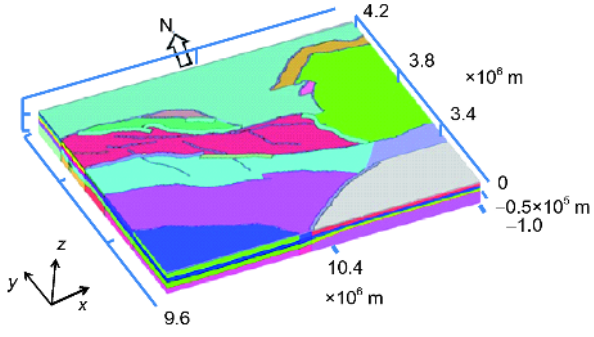

Figure 2 Three-dimensional finite element model of the eastern margin of the Tibetan Plateau.

discontinuous characteristics of faults on the northeastern Tibetan Plateau (He et al., 2013), and the assumption of a low friction coefficient is more consistent with the motion characteristics of the fracture zone over geological time. However, it is difficult to ensure convergence in such a complex fault model. According to Zheng et al. (2009), the deformation of the northeastern margin of the Tibetan Plateau is a distributed continuous deformation. Therefore, we use continuous medium of weak elements to describe the mechanical properties of active faults in this study, while also improving upon the efficiency of the calculations. Although the weak elements cannot reflect the interseismic deformation of active faults, the disturbance influence of historical earthquakes to the study area isn't considered in this paper, so using the weak elements to describe the faults is reasonable.

The crustal layer depth in the model was 100 km, and the model included five layers, consisting of the Earth's surface, upper crust, middle crust, lower crust, and uppermost mantle (Figure 3). The topography data used, ETOPO1, are from the American Geophysical Center (http://ngdc.noaa.gov/mgg/gdas/gd_designagrid.html), and they have a resolution of 1 s. Data on the layers of the crust (upper crust, middle crust, and lower crust) are from Stolk et al. (2013), who published a high-resolution velocity structure of Asia and its adjacent regions. The data of depth of Moho was obtained from the latest research data of Wang et al. (2017). Meshing the model with hexahedral elements, the average grid sizes of horizontal and vertical units in the crust was 4–5 km, the average grid size in the mantle was 4–5 km, and the vertical grid size was 10 km on average. The total number of the nodes was 948094, and the total number of elements in this model was 873600.

2.2 Material parameters

The numerical simulation was conducted by using the finite element software ADINA (ADINA R&D, Inc., June 2010). The physical equation of the model is a static equilibrium equation $\frac{\partial \sigma_{ij}}{\partial x_j} + f_i = 0$, where σ_{ij} are stress tensors, and f_i are the body forces. The Maxwell viscoelastic constitutive relation, which is one of the simplest viscoelastic materials, which was used in this study. Over geological time scales, the Maxwell constitutive relation is characterized by viscosity and elastic instantaneous performance. It can be used to simulate the ten thousand-year scale of the stress-strain evolution of the lithosphere, and the instantaneous elastic response of the lithosphere. The change in volume is elastic, and the shear deformation obeys the law of Maxwell viscoelasticity.

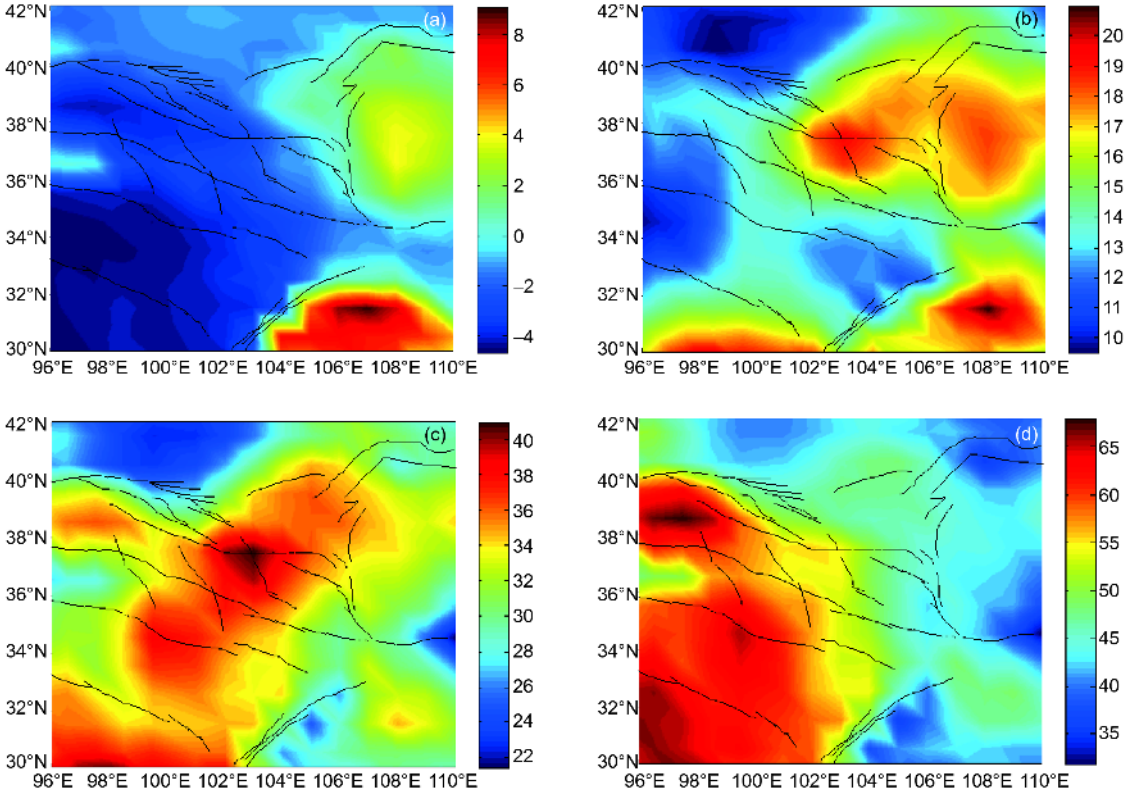

Figure 3 The depth in kilometers (km) of each layer in the model. (a) The surface of the upper crust; (b) the bottom of the upper crust; (c) the bottom of the middle crust; (d) the bottom of the lower crust.

Young's modulus is $E = v_p^2\rho(1+v)(1-2v)/(1-v)$ and Poisson's ratio is $v=\frac{1}{2}\left(\frac{v_P}{v_S}\right)^2 - 1 / \left(\frac{v_P}{v_S}\right)^2 - 1$, where v_P is P wave velocity, v_S is S wave velocity, and ρ is density. The P wave velocity of the upper crust, middle crust, lower crust, and upper mantle is shown in Stolk et al. (2013). The corresponding S wave velocity is shown in Li et al. (2013). Based on CRUST1.0 (http://igppweb.ucsd.edu/-gabi/ crust1.html), ρ is averaged. After calculations using formulas illustrated above, we obtained the Young's moduli of the surface, upper crust, middle crust, lower crust, and upper mantle of the Ordos block as 87, 87, 99, 118, and 169 GPa, respectively. The Young's moduli of the surface, upper crust, middle crust, lower crust, and upper mantle of the other blocks were 84, 84, 98, 111, and 169 GPa, respectively. The Young's modulus of the entire fault (considered continuously) was 10 GPa, which is nearly one order of magnitude smaller than those of the individual blocks. The Poisson's ratio did not exhibit significant differences in the horizontal direction; the Poisson's ratio of each block on the surface, upper crust, middle crust, lower crust, and upper mantle were 0.24, 0.24, 0.25, 0.26, and 0.28, respectively. The Poisson's ratio of the fault was 0.49, and the main purpose was to reduce the normal deformation of the fault, and to only consider its tangential deformation. The density of the surface, upper crust, middle crust, lower crust, and upper mantle of the blocks and the fault were 2700, 2700, 2850, 2930, and 3350 kg m^{-3}, respectively.

The rheological properties of different blocks in the Tibetan Plateau vary with depth (Shi and Cao, 2008; Sun et al., 2013), and they exhibit obvious lateral heterogeneity (Flesch et al., 2001; Wang and He, 2012). To reflect the differences in the lateral and vertical rheological properties of different blocks, the equivalent viscosity coefficient of material parameters of each model were provided by Sun et al. (2013), where the latest equivalent viscosity coefficient of the crust and upper mantle at different depths was calculated. The Erdos block, Alashan block, and Sichuan basin are all relatively stable, so their viscosity coefficients in the surface, upper crust, middle crust, lower crust, and upper mantle are 2.5×10^{21}, 5×10^{23}, 5×10^{23}, 1×10^{23} and 1×10^{22} Pa s, respectively. The viscosity coefficient of each layer of the Tibetan Plateau is 2×10^{20}, 3×10^{22}, 2×10^{21}, 4×10^{20} and 1×10^{21} Pa s, respectively. The viscosity coefficient of fault is 1×10^{21} Pa s.

2.3 Boundary conditions

Given the control of the dynamic boundary on the modern crustal movement in the northeastern margin of the Tibetan Plateau, the horizontal boundary load acting on the block boundary of the model was mainly considered for the interaction between the Indian plate and Eurasian plate. Li et al. (2012) analyzed the GPS data of the crustal movement recorded by an observation network in China, and obtained the crustal velocity field (relative to Eurasia) of the Chinese mainland and its adjacent area (Figure 4a). Here, we constrain boundary conditions using GPS data with respect to Eurasian plate. Boundary conditions were interpolated from the GPS velocities observed nearby (Figure 4b). Due to a lack of data support for the horizontal displacement rate of the deep lithosphere, three-dimensional boundary constraints were assumed to be invariant with depth. The surface of our model was also set as free. The bottom (at 100 km depth) was fixed in the vertical direction, and was free in the horizontal direction.

2.4 Initial conditions

The selection of initial conditions is one of the most difficult aspects of numerical simulations. The initial stress field cannot be obtained directly, but only through an inversion method; however, the state obtained is uncertain. Therefore, in this study, gravity was added to the model, and due to the long-term rheological properties of the lithosphere, the stress tended toward a lithostatic pressure state (i.e., a state of gravitational isostasy) (Yin, 1985). To consider the gravity of the crust and upper mantle in the initial stress state, we found

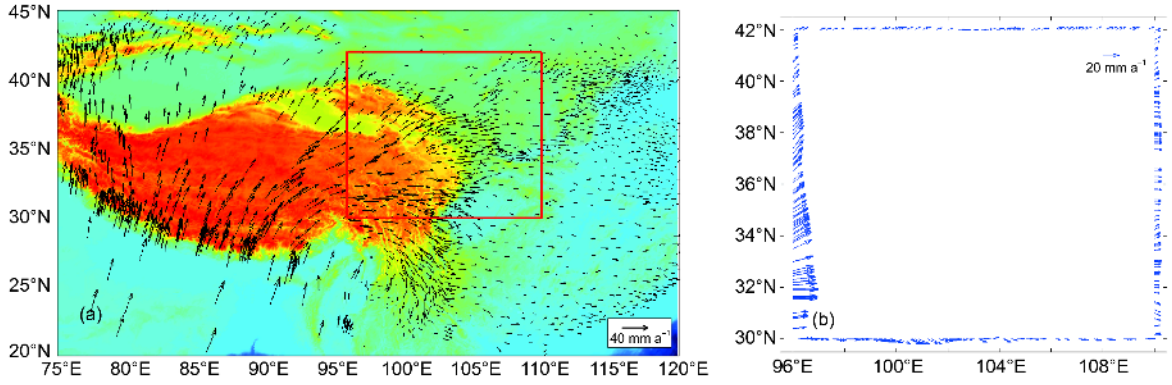

Figure 4 Boundary conditions. (a) The GPS data relative to the Eurasian plate obtained by Li et al. (2012); the red rectangle indicates the domain of our model; (b) velocity boundary conditions obtained by interpolation calculations provided by Li et al. (2012).

that after calculations for a period of 50000 years, the principal stresses in the three directions are close to the lithostatic pressure state. In Figure 5, we can see that the principal stress for the three directions of the observation point gradually approaches the same value, and it can be approximated to a stable state as the initial conditions of the model.

Using a new displacement elimination algorithm (*in situ* displacement removal), the initial displacement was removed and the grid was restored to the initial state. The crustal stress conditions remain the same after the elimination of the displacement, and the state is reflective of the current terrain, which is regarded as the initial stress of the model (Zhu et al., 2016). Then, horizontal boundary conditions were applied to simulate the interaction between blocks. After 100000 years loading, we obtained stable stress field and strain field as the background mechanical environment. In this calculation, the number of time steps was 100, and the time step size was 1000 years.

2.5 Mantle convection at the bottom of the model

Due to the higher resolution of regional seismic tomography models in characterizing transverse mantle structures, Zhu (2016) established a mantle convection model coupled with regional and global scale seismic velocity structures, and with the constraints of geoid anomalies and surface topography abnormalities to explore the influence of mantle convection on the stress field of the lithosphere in mainland China. Based on this convection model, a varying grid size was adopted in both horizontal and vertical directions. The depths of 0–100 km had a grid size of 1 km, depths of 100–670 km had a grid size of 10 km, depths of 670–1070 km had a grid size of 20 km, and depths of 1070–2900 km had a grid size of 36.6 km. In the horizontal direction across the region of (10°–60°N)×(65°–145°E), the grid size was 0.25°. The mantle convection and the velocity of mantle convection at the bottom of the lithosphere at a depth of 100 km are shown in Figure 6a and Figure 6b, respectively.

To quantitatively describe the effects of mantle convection on the lithospheric deformation of the northeastern margin of the Tibetan Plateau, we used the root mean square error (RMSE) to estimate the agreement between the simulated horizontal crustal deformation and the GPS observations. We interpolated the simulated velocity of the model surface to the GPS station within the model range used by Li et al. (2012), and then calculated the square root of the sum of

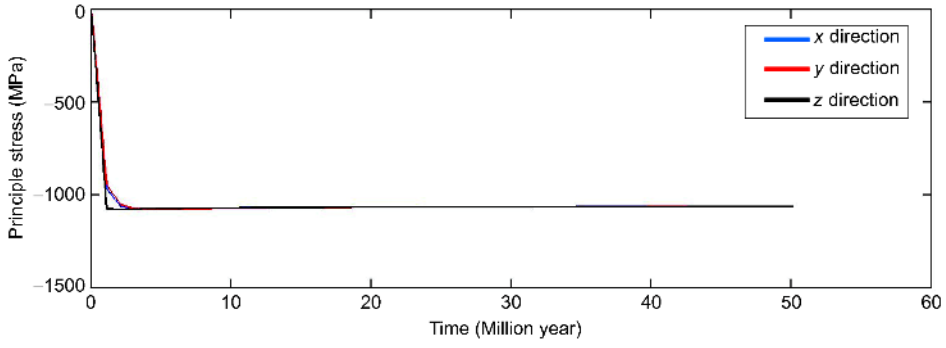

Figure 5 The principle stress curves of one surface node of the model versus the time.

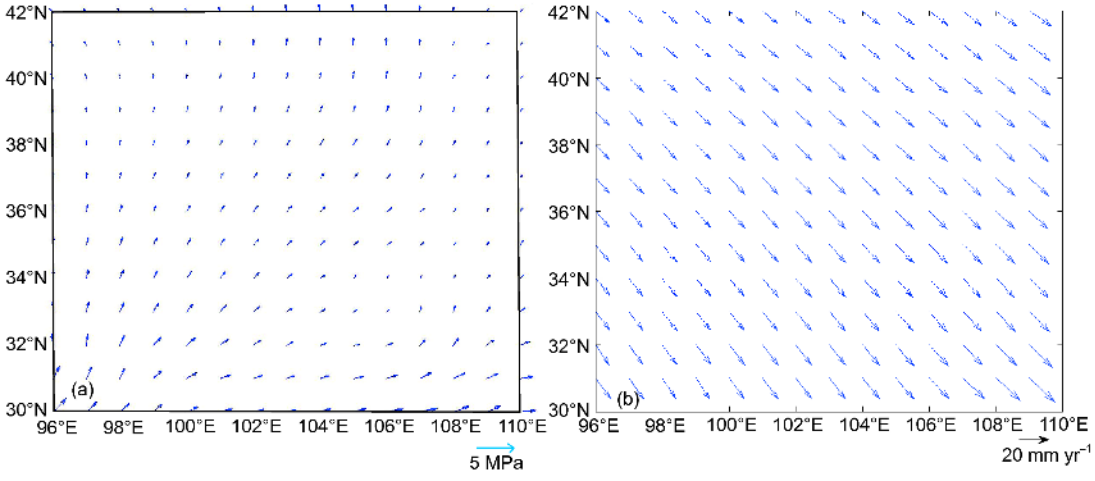

Figure 6 Deformation plots. (a) Mantle convection at a depth of 100 km; (b) the velocity of the mantle convection in the depth of 100 km.

squared deviations between the numerical results and the observations results from every GPS station by a ratio of N, which is the number of GPS stations; the formula is shown below in eq. (1). The coincidence between the simulation results and the observed results is indicated by σ, and if σ is small, the simulation results are closer to the actual observation results. A criterion for evaluating the deviation of simulation results (σ) was used, and the formula is shown as follows:

$$\sigma = \sqrt{\frac{\sum_{i=1}^{N}\left(V_{\mathrm{sim},i} - V_{\mathrm{obs},i}\right)^2}{N}}, \quad (1)$$

where σ is the RMSE between the simulated velocity of model surface and the GPS observations; N is the number of GPS stations used by Li et al. (2012), $V_{\mathrm{sim},i}$ is the interpolation of the simulated velocity of the model surface at the location of GPS station i, and $V_{\mathrm{obs},i}$ is the GPS-observed velocity at the location of GPS station i. The formula for calculating the deviation of the azimuth angle between simulation results and GPS-observed results is the same as eq. (1).

3. Results of numerical simulation

3.1 Results of numerical simulation without mantle convection

Considering the horizontal velocity boundary loading according to Li et al. (2012), and gravitational potential energy, but without considering mantle convection at the bottom of the model, we obtain the simulated crustal deformation of the model surface on northeastern margin of the Tibetan Plateau, which is illustrated as blue arrows in Figure 7, where the red arrows represent the observation GPS. From Figure 7, we can see that the simulated surface velocity and GPS observation are similar near the edge of the model. However, the simulated velocity direction in the western part of the Qilianshan block, and in the central area of the Qaidam block is east-west, while the velocity direction of GPS observations is north-east. For the eastern Bayanhar block near the Qaidam block, the simulated velocity direction is north-east to the east, which also differs from the GPS observations that exhibit a north-east direction only. In the eastern Bayanhar block near the Longmenshan fault zone, the direction of the simulated velocity of the surface is north-east, while the direction of GPS observations is southeast to east. To quantitatively describe compared simulation results with GPS observations, the RMSE shown in eq. (1) was calculated, and the difference of RMSE between the simulated surface velocity direction and observed GPS direction is 18.11°, and the difference of the RMSE between the simulated surface velocity and observed GPS is 0.78 mm yr^{-1} shown in Table 1. Overall, there is a clear difference between the simulated direction of crustal deformation and the ob-

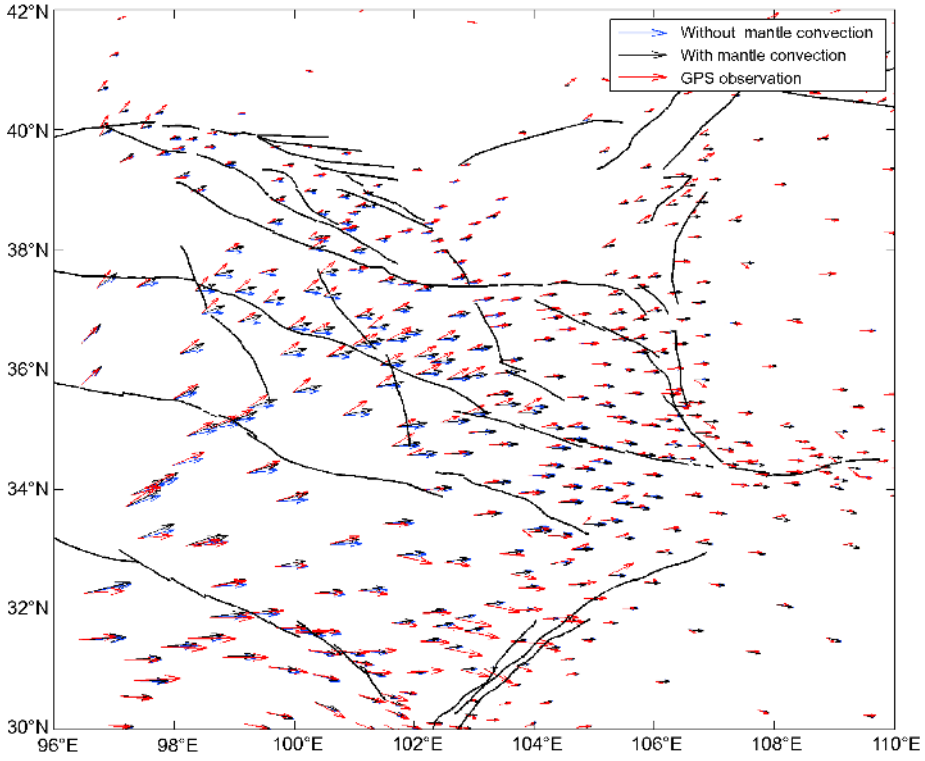

Figure 7 Comparison of calculated and observed (Li et al., 2012) horizontal crustal deformation rates. The red arrows are GPS observations, the blue arrows are the simulation results without applying mantle convection at the bottom of model, and the black arrows are the simulation results with mantle convection at the bottom of model with a mantle convection intensity factor of 1.

Table 1 Root mean square error (RMSE) between simulated and GPS-observed horizontal crustal deformation[a)]

Mantle convection imposing method	RMSE between the simulated and GPS-observed direction of horizontal crustal deformation (°)	RMSE between the simulated and GPS-observed rate horizontal crustal deformation (mm yr^{-1})
No mantle convection	18.1°	0.78
Mantle convection*	15.2°	0.72
Introduced mantle convection intensity factor	14.2°	0.72
Mantle convection**	17.52°	0.78

a) * Zhu, 2016; ** Xiong and Teng, 2002

served GPS direction.

3.2 Results of numerical simulation with mantle convection

Due to the fact that the simulated horizontal crustal deformation without mantle convection (i.e., the blue arrows in Figure 7) is quite different from the observed deformation (i.e., the red arrows in Figure 7), in addition to the interaction between blocks and the influence of gravity, there may also be other dynamic factors controlling the deformation behavior of the southeastern margin of the Tibetan Plateau. Bird et al. (2008) discussed the effect of small-scale mantle convection on controlling lithospheric movement, and some researchers (Zhang et al., 2007; Huang et al., 2008) have also considered mantle convection in their numerical simulations. After meta-analysis of published research findings, we considered not only block interactions and gravitational potential energy, but also mantle convection at the bottom of the model to evaluate the influence of mantle convection (Figure 6a) on the crustal movement of the northeastern margin of the Tibetan Plateau. Simulated results with mantle convection included are shown as black arrows in Figure 7. From this, we can see that for the area of the Qilianshan block, Helishan-Longshoushan tectonic belt, and Hexi Corridor basin in the north area of the Qilianshan and the central area of the Qaidam block, the direction of the simulated crustal deformation deflects ~15° from east-west to north, which is closer to the GPS-observed north-east direction. In the east area of the Bayanhar block, the difference between simulated results and the observed results is decreased by the addition of mantle convection at the bottom of the model. However, in the east of the Bayanhar block near the Longmenshan fault zone, the simulated direction of horizontal crustal deformation is north-east, which is still closer to the simulated results without mantle convection.

Based on the formula for RMSE (eq. (1)), we obtained the RMSE between the simulated horizontal crustal deformation direction with mantle convection at the bottom of the model and the direction observed by GPS (15.2°), and the RMSE between the simulated crustal deformation rate and the rate observed by GPS (0.72 mm yr^{-1}); these results are shown in Table 1. According to the results of the root mean square error, it can be found that, compared with direction of the observed GPS, the direction of the calculated crustal deformation in the northeastern margin of the Tibetan Plateau has certain improvement.

3.3 The simulated result introducing the mantle convection intensity factors

3.3.1 Mantle convection intensity factors

In the introduction of this paper, we postulated that in order to obtain the best bottom boundary load scheme, we should take into account the interactions between plate motions of certain velocities and the underlying convection material (i.e., account for differences in the degree of coupling between the lithosphere and asthenosphere among different blocks). An analysis of the crustal velocity fields of the Chinese continent and adjacent regions can be seen in Figure 4. Great differences between the rate of horizontal movement of different blocks in the simulation and the observed horizontal movement rates of the blocks for the Tibet Plateau are significantly higher than those of the Alashan block, Ordos block, and the southern China block (Sichuan basin). According to the findings of Zhu (2016), the depth of mantle convection is effectively the same in size and direction at a depth of 100 km in the model, which is approximately the southeast direction (Figure 6b). Therefore, we can see that the difference between the horizontal velocities of the northern area at a depth of 100 km in the Tibetan Plateau is significantly higher than that of the land around the plateau. Based on the results of Bourne et al. (1998), the mantle convection intensity of the internal block of the Tibetan Plateau should also be significantly greater than the intensities of the adjacent areas.

The mantle convection intensity factor is determined based on the theory of vertically coherent deformation of the lithosphere (Flesch et al., 2005; Chang et al., 2017). If the lithosphere from the top to the bottom does not exhibit characteristics of vertically coherent deformation, then the local, small-scale mantle convection applied to the bottom of the lithosphere can be neglected (i.e. the mantle convection intensity factor can be set to 0). However, if the lithosphere from the top to the bottom exhibits characteristics of vertically coherent deformation, then the local, small-scale

mantle convection applied on the bottom of the lithosphere must be considered. Combined with analysis of the surface deformation and shear wave splitting data, Chang et al. (2017) obtained some results, in which we can see that the fast wave directions in the interior of the Tibetan Plateau and Alashan block are consistent with the fast wave directions predicted by the surface deformation field. Chang et al. (2017) also found that the surface deformation field was consistent with the mantle deformation field, and the crust was strongly coupled to the lithosphere mantle, and it consistent with the vertical coherent deformation characteristics of the lithosphere. However, in the Ordos block and Sichuan basin, the fast wave direction among most measuring points is inconsistent with the surface deformation field, and the time delay relative to other tectonic units is very small. They also exhibit weak anisotropic characteristics, reflecting the internal rigidity of the Ordos block and the Sichuan basin, which do not exhibit vertically coherent deformation characteristics. For the purposes of this study, mantle convection for these sections can be neglected (i.e., their intensity factors can be set to 0). As for each block in the Tibet Plateau, Because of the large differences in deformation velocity between the upper and lower layers of the Tibet Plateau, the corresponding intensity factor of Tibet Plateau is set to be ratio of the velocity difference between the upper and lower layers.

3.3.2 *The results of the simulation*

After comparative analyses of the above two sections (Figure 7), it became clear that the dynamic factors controlling the crustal movement pattern is very complex. To obtain simulation results that are closer to the GPS observations (Bourne et al., 1998), we derived a convection intensity factor of 8 for the Bayan block, Qaidam block, and the central Qilianshan using the error testing method, where the difference between the surface movement rate and mantle convection rate is the largest. The specific calculations and discussions are seen in section 4.1 below. The best simulation result with included mantle convection intensity factors is shown in Figure 8 and Table 1. The best intensity factor schema are shown as follows: an intensity factor of 8 for the Bayan block, Qaidam block and the central Qilianshan, an intensity factor of 1 for the east of Bayanhar block, Alashan block, eastern Qilianshan block, eastern Qaidam block, Sichuan-Yunnan block, and Hexi Corridor basin, and an intensity factor of 0 for the Ordos block and southern China block (Sichuan basin).

In Figure 8, we can see that the direction of the simulated horizontal crustal deformation (the blue arrows) deflects ~40° from east-west to north in the area of the Qilianshan block, the Helishan-Longshoushan tectonic belt, and the

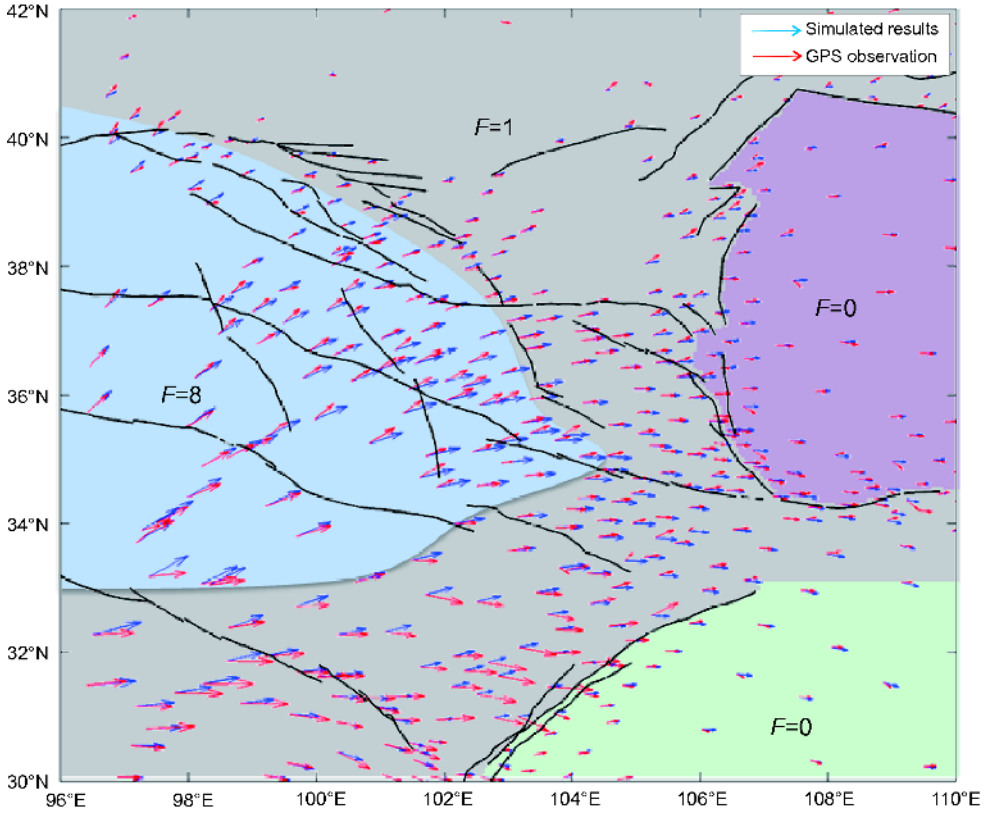

Figure 8 Comparison of calculated and observed (Li et al., 2012) horizontal crustal deformation rates considering the mantle convection intensity factor (*F*).

Hexi Corridor basin north of Qilianshan and the central area of the Qaidam block. These results are nearly consistent with GPS observations that reveal a north-east direction (the red arrows). When applying the mantle convection intensity factor at the bottom of the model for the eastern area of Bayanhar block, the simulated results are consistent with the observed results. Due to mantle convection, the direction of horizontal crustal deformation in the eastern Bayanhar block near the Longmenshan fault zone deflects to the northeast, and there are subsequently large differences between the simulated results and the GPS observations. One possible reason for this is that the Longmenshan fault zone turned from its previous locked position into a sliding state after the 2008 M_S8.0 Wenchuan earthquake. According to the GPS observations, after the Wenchuan earthquake, crustal deformation in this area changed dramatically. Since that time, the rate of the crustal deformation has increased significantly, and the direction of crustal deformation changed to some extent. Because the upheaval of the Wenchuan earthquake is not taken into account in the paper, the associated movement of the crust cannot be reflected.

From the overall analysis (third row of Table 1), it can be seen that, relative to the simulated results without mantle convection (first row of Table 1), the RMSE of the direction of horizontal crustal deformation between the simulation and GPS observations decreases by 4°, and the RMSE of the rate of crustal deformation between the simulation and the GPS observations decreases by 0.06 mm yr^{-1}.

3.4 Testing stress state in the middle crust

Using numerical simulation, we studied the stress and stain states of the northeastern margin of the Tibetan Plateau under the effect of mantle convection, gravitational potential energy of plateau, and the interaction among blocks, and obtained the maximum principal stress direction and distribution of the principal stress (the cloud map) for the middle crust (10–20 km depth). We then compared these findings to the latest world stress map published in 2008, which is based on focal mechanism solutions and *in situ* stress measurements (Heidbach et al., 2010). In Figure 9, we can see that, in the northern region of the northeastern margin of the Tibetan Plateau, the direction of the maximum principal compressive stress in the horizontal direction is NE-SW, which is consistent with the direction of the horizontal compressive stress observed by GPS. This is caused by the movement of plateau material to the north-east, and it is hindered by the Alashan and Erdos blocks. In the eastern margin of the Tibetan Plateau, the overall pattern of the maximum principal stress direction in the study area is radial, and centered on the Tibetan Plateau. The numerical simulation results of the maximum principal compressive

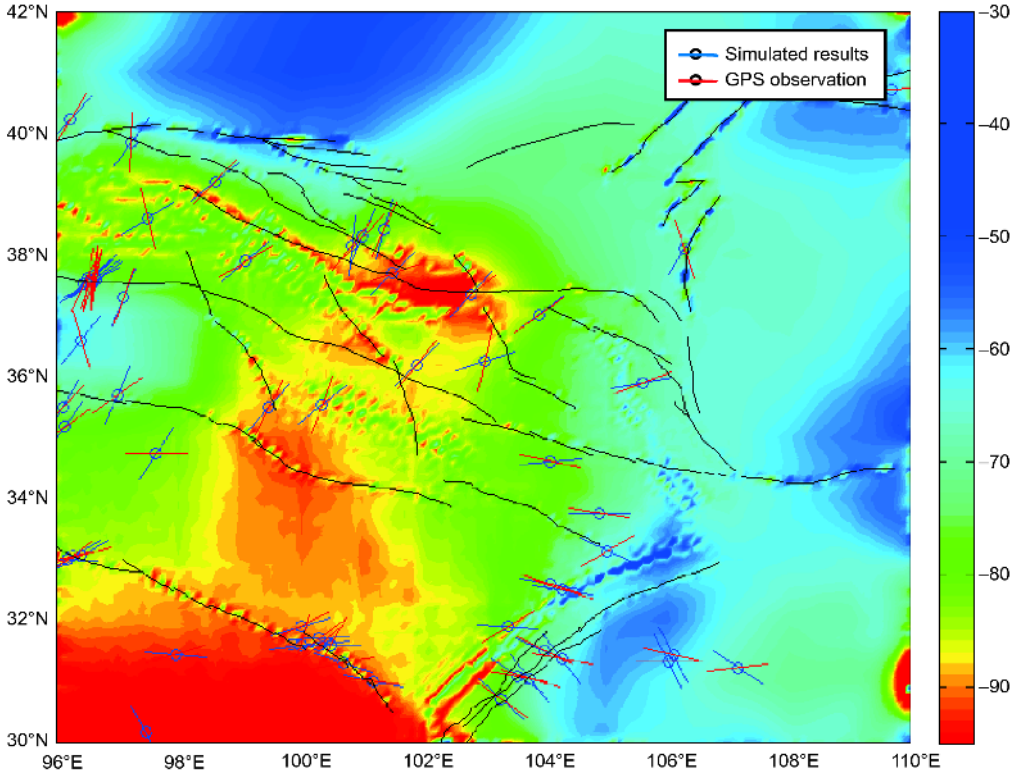

Figure 9 Comparison of calculated and observed maximum principal stress direction and distribution of the principle stress (the cloud map) in the middle crust.

stress direction obtained for the middle crust are dominantly consistent with the world stress distribution map (Heidbach et al., 2010) in the study area.

The maximum principle stress is shown as cloud in Figure 9. Here, we can see that the northeastern margin of the Tibetan Plateau is in a state of compression, wherein stress is greater in the west than in the east, and that stress is mainly concentrated in the area of Tibetan Plateau, the high terrain area around the basin and near the fault. In the eastern region of the northeastern margin of the Tibetan Plateau stress is ~40–50 MPa, and in the Tibetan Plateau interior, it can reach 80–90 MPa; this is consistent in magnitude with Chinese stress distribution results obtained by Li et al. (2002) and Zheng et al. (2006). We can see that the principal compressive stress of the Sichuan-Yunnan block is compressive and the direction is rotated from the east to the southeast. The principal stress directions in the Sichuan basin and Erdos block are south-east and east-southeast, respectively, and the principal stress is mainly compressive, though, the values of the stress are relatively small and evenly distributed. The principal stress direction in the Qaidam basin is north-east, and the principal stress is mainly compressive. The value of the stress in the local area of the Qaidam basin is small; however, the compressive stress around the Qaidam basin is strong; Lastly, the values of the stress in some other areas near the fault zone, including the Qilianshan fault zone, Riyueshan fault zone, the east of the Kunlunshan fault zone, and the south of the Longmenshan fault zone are very high.

We believe that the main reason for the stress field distributions described above is the extrusion effect of the Indian plate, which has resulted in a high-pressure stress environment in the Tibetan Plateau. Secondly, because the high terrain of the Tibetan Plateau has high gravity, resulting in extrusion of plateau material outward, at the same time blocked by the Sichuan basin and the Yangtze block, resulting the direction of the maximum principal stress in the study area presents a radiative image centered on the Tibetan Plateau. Finally, the direction of the mantle convection at the bottom of the lithosphere appears to drive the extruded materials to turn from north to east.

4. Discussion and conclusions

4.1 Determination of mantle convection intensity factors

Determining the stress intensity factor is mainly based on the following three aspects: (1) Zhu (2017) proposed that plate motion has an important impact on the speed and shape of mantle convection; (2) Bourne et al. (1998) proposed that the force from the underlying rock layer that the crust can withstand is proportion to the horizontal velocity of the upper and lower layers of the crust; and (3) The theory behind the significant differences in lithospheric characteristics of vertically coherent deformation on the Tibetan Plateau, which are shown in Flesch et al. (2005) and Chang et al. (2017).

From the comparison of the simulated crustal deformation and the GPS observations shown in Figure 7, we can see that in the part of the Tibetan Plateau area that includes the Qilianshan block, the Qaidam block, and the eastern area of Bayanhar block close to the Qaidam block, the difference between the direction of the simulated crustal deformation and GPS observations is obvious. Based on the findings of Chang et al. (2017), the mantle convection intensity factor at the bottom of model in the area of Sichuan basin and the Erdos block is 0. Because the simulated crustal deformation in the area of Sichuan-Yunnan, Alashan block, and the Bayanhar block is consistent with the GPS observations, the intensity factor of the mantle convection is 1. We applied many mantle convection intensity factors to the bottom of the northeast of Tibetan Plateau, and using GPS observations as the constraint, we obtained the RMSE between the simulated crustal deformation and GPS-observed deformation in both the rate and azimuth. From this, we determined the best mantle convection intensity factor by the error testing method, and the RMSEs with different intensity factors are shown in Figure 10. From Figure 10a, it can be seen that when the mantle convection intensity factor is between 6 and 8, the RMSE of the simulated direction of crustal deformation and the GPS-observed deformation is minimized. From Figure 10b, it can be seen that when the mantle convection intensity factor is between 8 and 10, the RMSE of the rate of simulated crustal deformation and the GPS-observed deformation is also minimized. Based on these findings, we chose the mantle convection intensity factor in the domain of Tibetan Plateau (shown in Figure 8) as 8 to ensure that the RMSE of both the direction and the rate of the simulated and GPS-observed crustal deformation are relatively small.

Xu et al. (2006) proposed that the rise of Qilianshan in the northern margin of the Tibetan Plateau was the result of the effect of a high extrusion rate on the material inclined extrusion. The influence of the lower crust melt on the rheological properties of the lower crust, and the drive of material extrusion style and mode may be the deep dynamic sources of rapid extrusion in this area. Zhang et al. (2013) noted that under the dynamic action of plate extrusion and intraplate mantle convection, the rigid block movement and the non-rigid continuous deformation of the upper crust were all surficial responses to deep, viscoplastic flow. The findings of Yuan et al. (2004) also suggested that the deformation mode of the northeastern margin of the Tibetan Plateau was complex, and a simple model could not comprehensively summarize. At the same time, considering the horizontal interaction among blocks, combined with the influence of mantle convection at the bottom of the lithosphere, may provide a more reasonable explanation for the distribution of

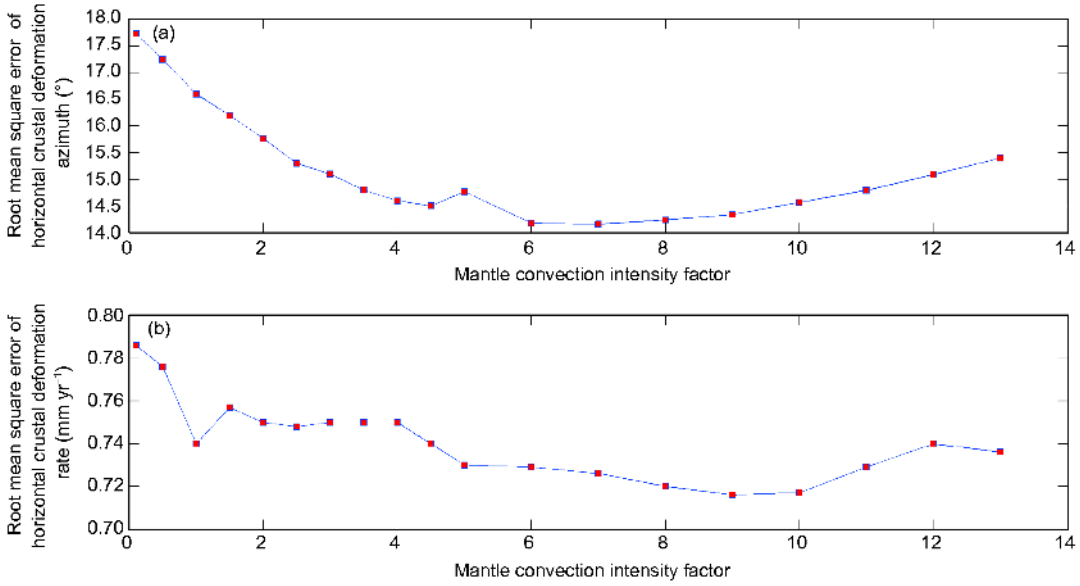

Figure 10 RMSE between the simulated and GPS-observed results under different mantle convection intensity factors.

characteristics in this remarkable deformation mode. Based on the above research, this study elaborates on the ideas of Flesch et al. (2005) and Chang et al. (2017) about differences in the coupling degree between the asthenosphere and lithosphere, and the coupling degree of the crust and upper mantle, using the mantle convection intensity factor to describe the strong coupling of the crust and upper mantle in the northeast of Tibetan Plateau caused by vertically coherent deformation. Meanwhile, the Huanan block and the central of the Erdos block do not exhibit vertically coherent deformation. The methods we present here offer a new framework for studying the complex, deeply driven deformation in the Tibetan Plateau and its surrounding areas.

In this study, the simulated results were closer to the observed results when the mantle convection intensity factor in the northeastern margin of the Tibetan Plateau was between 8 and 10, which is much higher than for either the Erdos block or the Huanan block. This can provide a deep driving force for the existence of high extrusion rate, high strain energy accumulation rate and strong earthquake frequency in Qilianshan area, and also using forward method of error testing confirms difference of vertical coherent deformation of lithosphere found by seismic wave anisotropy. From these geodynamic analyses, we can infer that the bottom of the northeastern margin of the Tibetan Plateau is likely characterized by strong mantle convection.

Mantle convection was applied to the bottom of the model, and at a depth of 100 km in this study, and the fluctuation of the bottom surface was not taken into account. Finally, horizontal mantle convection was applied, and vertical mantle convection was not considered; the further research to account for these factors will be conducted in the future.

4.2 Numerical simulation on the mantle convection obtained by different methods

The establishment of mantle convection model had obvious progress in the resolution by using seismic tomography method, therefore, the convection model of Zhu (2016) was chosen for this study. However, in order to compare the effects of different methods of mantle convection with the current tectonic movement along the northeastern margin of the Tibetan Plateau, the mantle convection obtained by Xiong and Teng (2002) was applied at the bottom of the model and used for calculating the simulation results of horizontal crustal deformation shown in Figure 11. Here, we can see that the results of these two different convection models are different, especially for the interior of the Tibetan Plateau. Comparing the results of the simulated crustal deformation using the convection models of Zhu (2016) and Xiong and Teng (2002), we can see that the mantle convection obtained by Zhu (2016) drives the direction of the simulated crustal deformation to deflect northward by ~15°, which is close to the GPS observations. At the same time, the RMSE of the simulated value and the observed value was compared (Table 1). From this, we can see that the simulation results of the Zhu (2016) method are closer to the GPS observation results than the results of simulation using the method of Xiong and Teng (2002).

Through the comparison of two typical small scale convection model and regional tectonic movement observation results, we can see the value of these models and their existence of uncertainty. The mantle convection stress field calculated by Xiong and Teng (2002) was consistent with the surface movements of the northeastern Tibetan Plateau,

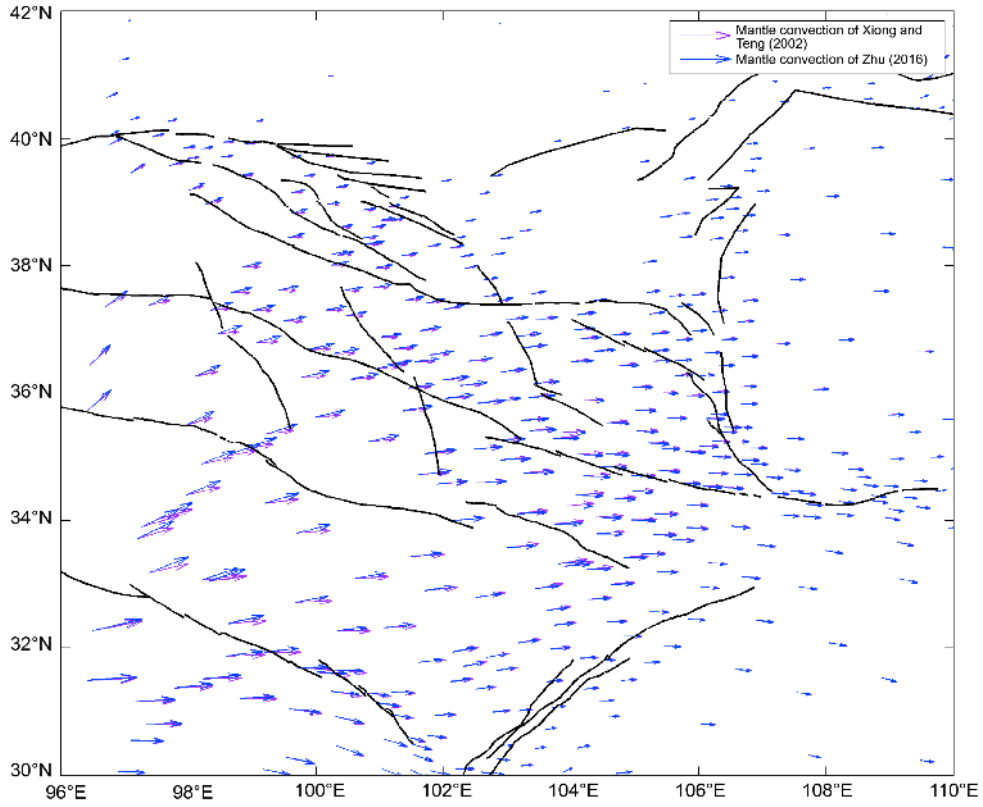

Figure 11 Comparison of calculated horizontal crustal deformation rates between different mantle convection models.

while the correspondence between them was poor in the adjacent areas. This research also tried to explain the coincidence of the simulated and observed results via decoupling of the crust and the mantle. Small-scale mantle convection was calculated by Zhu (2016) using seismic tomography data, and the directions of the convection stress were dominantly consistent with the GPS observations in the Tibetan Plateau and its eastern and northern marginal areas. In the northeastern margin of Erdos platform and junction area, the mantle convection stress direction is from south to north. In the Ordos platform, the direction of the mantle convection stress is NNE, and there are large differences between the crustal movement calculations and the GPS observations. In order to study the effect of mantle convection on crustal deformation, we need to gather more reliable data on mantle convection. In this study, the latest available mantle convection data was used, and the simulation results revealed that applying mantle convection may still improve geodynamic models of the northeastern margin of the Tibetan Plateau.

4.3 Conclusions

Based on the three-dimension viscoelastic finite element method, in consideration of complex terrain of the northeastern margin of Tibetan Plateau and its adjacent areas, the boundary compression conditions interpolation by GPS data, and the difference of mechanical properties (strength) in the depth of the crust based on recently published boundary compression detection results, we simulated the horizontal crustal deformation under different mantle convection schemes, and compared our findings with the published observational data of Li et al. (2012). Further, we investigated the possible controlling effect of mantle convection on the deformation of the lithosphere in the northeastern margin of the Tibetan Plateau. According to the results of the simulation, we can see that as follows:

Our results indicate that the interaction between blocks as well as high altitude gravity play significant roles in controlling the patterns of crustal movement along the southeastern margin of Tibetan Plateau. Crustal movement gradually decreases from the interior to the edge of plateau; however, the movement characteristics of the north-east direction in the interior of the Tibetan Plateau are not reflected. This is especially true for the central area of Qilianshan block and Qaidam block, where it can be seen that the direction of movement within the Tibetan Plateau is affected by other dynamic factors. By applying mantle convection and the mantle convection intensity factor, the results of simulated and GPS-observed are more consistent, which suggests that mantle convection at the bottom of the lithosphere has a controlling effect on the crustal deformation direction inside

the Tibetan Plateau. More specifically, in the area of the Qilianshan block, the Helishan-Longshoushan tectonic belt, the Hexi Corridor basin to the north of Qilianshan and the central area of the Qaidam block, mantle convection under the lithosphere of the Tibetan Plateau make the direction of the simulated horizontal crustal deformation deflect by ~40° from east-west to north. At the same time, it causes the direction of the crustal deformation in the Bayanhar block to deflect to north by 10°–15°. From the tectonic map, it can be seen that the Qaidam block and the north boundary of Qilianshan block form a series of thrust faults, including the northern margin fault in the Qaidam basin, Xiangshan-Tianjingshan fault, Qilianshan-Beiyuan fault, and the Haiyuan fault. There is an obvious relationship between the formation of thrust faults and the effect of mantle convection on the direction of crustal movement in Tibetan Plateau.

When considering the mantle convection intensity factor, according to the seismic anisotropy research of Chang et al. (2017), the strength of the vertical coherence deformation was significantly different between the Tibetan Plateau and its adjacent areas; this may also be related to differences in the degree of coupling degree of the lithosphere and the asthenosphere. To determine how the degree of coupling may affect the mantle and crust in the region of Tibetan Plateau, vertically coherent deformation must be considered. Using the RMSE to determine the best mantle convection intensity factor, which causes the simulated crustal deformation of the Tibetan Plateau to be more consistent with the GPS observation, our findings further support the results of Chang et al. (2017) (i.e., that the deformation mode in the northeast of the Tibetan Plateau is vertically coherent deformation, and that the crust and mantle are strongly coupled). Therefore, we must consider the difference strengths of each block relative to mantle convection in the Tibetan Plateau when conducting simulations.

The numerical simulation results also verify the idea of some research (Liu and Yang, 2003; Bird et al., 2008) as follows: high altitude terrain accumulation of gravity, Complex physical and mechanical properties of lithosphere, the interaction of the blocks and mantle convection jointly control the crustal movement of lithosphere in the northeastern margin of Tibetan Plateau. However, there are still some factors that have not yet been considered, including the erosion of the surface and the disturbance of regional stress patterns caused by strong earthquakes. For example, the 2008 M_S8.0 Wenchuan earthquake, which caused the surface movement rate of Longmenshan area to double, and this led to the differences reported between the simulated crustal deformation and the GPS observations in the Longmenshan area. In order to determine the most important factors that dominate the overall trends in crustal movement in the Tibetan Plateau, further research that accounts for these factors is needed.

Acknowledgements *We thank Professors Xiong Xiong, Yuan Daoyang, Tang Fangtou, and Chang Lijun, three anonymous reviewers, and the chief editor for their useful suggestions. We used Moho depths data calculated by Dr. Wang Xingchen and Prof. Ding Zhifeng, the crustal structure data of Stolk (2013), and the P and S wave velocity data of Li Yonghua (2013). We express our sincere thanks to the providers of these data. This study was supported by the National Natural Science Foundation of China (Grant No. 41504079), and the China National Special Fund for Earthquake Scientific Research in Public Interest (Grant No. 201308011).*

References

ADINA R& D. Inc. June 2010. Theory and Modeling Guide Volume I: ADINA, Report ARD 10–7

Becker T W, Faccenna C. 2011. Mantle conveyor beneath the Tethyan collisional belt. Earth Planet Sci Lett, 310: 453–461

Bird P. 1999. Thin-plate and thin-shell finite-element programs for forward dynamic modeling of plate deformation and faulting. Comput Geosci, 25: 383–394

Bird P, Liu Z, Rucker W K. 2008. Stresses that drive the plates from below: Definitions, computational path, model optimization, and error analysis. J Geophys Res, 113: B11406

Bourne S J, England P C, Parsons B. 1998. The motion of crustal blocks driven by flow of the lower lithosphere and implications for slip rates of continental strike-slip faults. Nature, 391: 655–659

Chang L J, Ding Z F, Wang C Y, Flesch L M. 2017. Vertical coherence of deformation in lithosphere in the NE margin of the Tibetan plateau using GPS and shear-wave splitting data. Tectonophysics, 699: 93–101

Chen L, Capitanio F A, Liu L, Gerya T V. 2017. Crustal rheology controls on the Tibetan plateau formation during India-Asia convergence. Nat Commun, 8: 15992

Chen Y T, Yang Z X, Zhang Y, Liu C. 2013. From 2008 Wenchuan earthquake to 2013 Lushan earthquake (in Chinese). Sci China Earth Sci, 43: 1064–1072

Cui D X, Wang Q L, Hu Y X, Wang W P, Liang W F. 2009. Lithosphere deformation and deformation mechanism in northeastern margin of Qinghai-Tibet plateau (in Chinese). Chin J Geophys, 52: 1490–1499

Faccenna C, Becker T W, Conrad C P, Husson L. 2013. Mountain building and mantle dynamics. Tectonics, 32: 80–93

Fang Y, Jiang Z S, Zhang J, Wu Y Q. 2009. High-resolution characteristics of recent crustal movement in Qinghai-Tibet Plateau (in Chinese). Earth Sci—J China Univ Geosci, 34: 399–404

Flesch L M, Haines A J, Holt W E. 2001. Dynamics of the India-Eurasia collision zone. J Geophys Res, 106: 16435–16460

Flesch L M, Holt W E, Silver P G, Stephenson M, Wang C Y, Chan W W. 2005. Constraining the extent of crust-mantle coupling in central Asia using GPS, geologic, and shear wave splitting data. Earth Planet Sci Lett, 238: 248–268

Fu R S, Huang J H, Xu Y M, Chang X H. 1998. Study of the mantle dynamics of the lithosphere movements in the region from Qinghai-Xizang plateau to Tianshan mountain (in Chinese). Chin J Geophys, 41: 658–668

Fu R S, Huang J H, Dong S Q, Zhang Q S, Chang X H. 2003. A new mantle convection model constrained by seismic tomography data (in Chinese). Chin J Geophys, 46: 772–778

Fu R S, Wang J Y, Chang X H, Huang J H, Dai Z Y, Zha X J. 2005. Upper mantle convection driving by density anomaly and a test model (in Chinese). Acta Seismol Sin, 27: 25–32

Ge W P, Wang M, Shen Z K, Yuan D Y, Zhen W J. 2013. Intersiesmic kinematics and deformation patterns on the upper crust of Qaidam-Qilianshan block (in Chinese). Chin J Geophys, 56: 2994–3010

Hao M, Qin S L, Li Y H, Chang X H. 2014. Recent horizontal velocity field of north eastern Tibetan plateau (in Chinese). J Geod Geody, 34: 99–103

He J K, Lu S J, Wang W M. 2013. Three-dimensional mechanical modeling

of the GPS velocity field around the northeastern Tibetan plateau and surrounding regions. Tectonophysics, 584: 257–266
Heidbach O, Tingay M, Barth A, Reinecker J, Kurfeß D, Müller B. 2010. Global crustal stress pattern based on the World Stress Map database release 2008. Tectonophysics, 482: 3–15
Huang J, Zhong S. 2005. Sublithospheric small-scale convection and its implications for the residual topography at old ocean basins and the plate model. J Geophys Res, 110: B05404
Huang J P, Fu R S, Zheng Y, Xue T X, Liu X, Han L B. 2008. The influence of mantle convection on the lithospheric deformation of China mainland. Chin J Geophys, 51: 733–743
Li Q, You X Z, Yang S M, Du R L, Qiao X J, Zou R, Wang Q. 2012. A precise velocity field of tectonic deformation in China as inferred from intensive GPS observations. Sci China Earth Sci, 55: 695–698
Li Y H, Cui D X, Hao M. 2015. GPS-constrained inversion of slip rate on major active faults in the northeastern margin of Tibet Plateau (in Chinese). Earth Sci—J China Univ Geosci, 40: 1767–1780
Li Y H, Wu Q J, Pan J T, Zhang F X, Yu D X. 2013. An upper-mantle S-wave velocity model for East Asia from Rayleigh wave tomography. Earth Planet Sci Lett, 377-378: 367–377
Li Z N, Fu R S, Huang J H. 2002. Numerical simulation of the Qinghai-Xizang plateau uplift under the effect of denudation and mantle convection (in Chinese). Chin J Geophys, 45: 516–524
Liang S M, Gan W J, Shen C Z, Xiao G R, Liu J, Chen W T, Ding X G, Zhou D M. 2013. Three-dimensional velocity field of present-day crustal motion of the Tibetan Plateau derived from GPS measurements. J Geophys Res-Solid Earth, 118: 5722–5732
Liu M, Yang Y Q. 2003. Extensional collapse of the Tibetan Plateau: Results of three-dimensional finite element modeling. J Geophys Res, 108: 2361
Shi Y L, Cao J L. 2008. Effective viscosity of China continental lithosphere (in Chinese). Earth Sci Front, 15: 82–95
Steinberger B, Schmeling H, Marquart G. 2001. Large-scale lithospheric stress field and topography induced by global mantle circulation. Earth Planet Sci Lett, 186: 75–91
Stolk W, Kaban M, Beekman F, Tesauro M, Mooney W D, Cloetingh S. 2013. High resolution regional crustal models from irregularly distributed data: Application to Asia and adjacent areas. Tectonophysics, 602: 55–68
Sun Y J, Deng S W, Fan T Y, Zhang H, Shi Y L. 2013. 3D rheological structure of the continental lithosphere beneath China and adjacent regions (in Chinese). Chin J Geophys, 56: 2936–2946
Teng J W, Bai D H, Yang H, Zhang H S, Zhang Y Q, Yan Y F, Ruan X M. 2008. Deep processes and dynamic responses associated with the Wenchuan M_S8.0 earthquake of 2008 (in Chinese). Chin J Geophys, 51: 1385–1402
Wang X C, Li Y H, Ding Z F, Zhu L P, Wang C Y, Bao X W, Wu Y. 2017. Three-dimensional lithospheric S wave velocity model of the NE Tibetan Plateau and western North China Craton. J Geophys Res-Solid Earth, 122: 6703–6720
Wang X F, He J K. 2012. Channel flow of the lower crust and its relation to large-scale tectonic geomorphology of the eastern Tibetan Plateau. Sci China Earth Sci, 55: 1383–1390
Xiong X, Teng J W. 2002. Study on crustal movement and deep process in eastern Qinghai-Xizang Plateau (in Chinese). Chin J Geophys, 45: 507–515
Xiong X, Fu R S, Teng J W, Xu H Z. 2005. A study of mantle dynamics of the tibetan plateau (in Chinese). Adv Earth Sci, 20: 970–979
Xiong X, Shan B, Wang J Y, Zheng Y. 2010. Small-scale upper mantle convection beneath the Mongolia-Baikal rift zone and its geodynamic significance. Chin J Geophys, 53: 529–541
Xu T, Wu Z B, Zhang Z J, Tian X B, Deng Y F, Wu C J, Teng J W. 2014. Crustal structure across the Kunlun fault from passive source seismic profiling in East Tibet. Tectonophysics, 627: 98–107
Xu Z Q, Yang J S, Li H B, Zhang J X, Zeng L S, Jiang M. 2006. The Qinghai-Tibet plateau and continental dynamics: A review on terrain tectonics, collisional orogenesis, and processes and mechanisms for the rise of the plateau (in Chinese). Geol China, 33: 221–238
Yuan D Y, Zhang P Z, Liu B C, Mao F Y, Gan W J, Wang Z C, Zheng W J, Guo H. 2004. Geometrical imagery and tectonic transformation of late quaternary active tectonics in northeastern margin of Qinghai-Xizang Plateau (in Chinese). Acta Geol Sin, 78: 270–278
Yin X C. 1985. Solid Mechanics (in Chinese). Beijing: Seismological Press
Zhang D N, Yuan S Y, Shen Z K. 2007. Numerical simulation of the recent crust movement and the fault activities in Tibetan Plateau (in Chinese). Chin J Geophys, 50:153–162
Zhang P Z, Deng Q D, Zhang G M, Ma, Gan W J, Min W, Mao F Y, Wang Q. 2003. Active tectonic blocks and strong earthquakes I the continent China. Sci China Ser D-Earth Sci, 46 (Suppl):13–24
Zhang P Z, Deng Q D, Zhang Z Q, Li H B. 2013. Active faults, earthquake hazards and associated geodynamic processes in continental China (in Chinese). Sci China Earth Sci, 43: 1607–1620
Zheng W J, Zhang P Z, Yuan D Y, Zheng D W. 2009. Deformation on the northern of the Tibetan plateau from GPS measurement and geologic rates of Late Quaternary along the major fault (in Chinese). Chin J Geophys, 52: 2491–2508
Zheng Y, Fu R S, Xiong X. 2006. Dynamic simulation of lithospheric evolution from the modern China mainland and its surrounding areas (in Chinese). Chin J Geophys, 49: 415–427
Zhu A Y, Zhang D N, Jiang C S. 2016. Numerical simulation of the segmentation of the stress state of the Anninghe-Zemuhe-Xiaojiang faults. Sci China Earth Sci, 59: 384–396
Zhu T. 2014. Tomography-based mantle flow beneath Mongolia-Baikal area. Phys Earth Planet Inter, 237: 40–50
Zhu T. 2016. Lithospheric stress and uppermantle dynamics in mainland China due to mantle flow based on combination of global- and regional-scale seismic tomography. J Asian Earth Sci, 132: 103–117
Zhu T. 2017. Effects of Eurasian plate motions on mantle convective velocity and horizontal shear stress fields at the base of the lithosphere beneath Mainland China (in Chinese). Geosci Front, 24: 192–206

(Responsible editor: Ling CHEN)